The Pseudospectral Time-Domain (PSTD) Algorithm for Acoustic Waves in Absorptive Media

Qing Huo Liu, *Senior Member, IEEE*

***Abstract*—A technique based on the combination of Fourier pseudospectral method and the perfectly matched layer (PML) is developed to simulate transient acoustic wave propagation in multidimensional, inhomogeneous, absorptive media. Instead of the finite difference approximation in the conventional finite-difference time-domain (FDTD) method, this technique uses trigonometric functions, through an FFT (fast Fourier transform) algorithm, to represent the spatial derivatives in partial differential equations. Traditionally the Fourier pseudospectral method is used only for spatially periodic problems because the use of FFT implies periodicity. In order to overcome this limitation, the perfectly matched layer is used to attenuate the waves from other periods, thus allowing the method to be applicable to unbounded media. This new algorithm, referred to as the pseudospectral time-domain (PSTD) algorithm, is developed to solve large-scale problems for acoustic waves. It has an infinite order of accuracy in the spatial derivatives, and thus requires much fewer unknowns than the conventional FDTD method. Numerical results confirms the efficacy of the PSTD method.**

I. Introduction

The finite-difference time-domain (FDTD) method has been very successful in solving time-dependent partial differential equations, including those arising from acoustic wave propagation in inhomogeneous media. For acoustic waves, one can start with either a second-order partial differential equation for the pressure field, or a set of coupled equations for the pressure and particle velocity fields. In the second-order finite-difference method, the most commonly used FDTD method, both the spatial and temporal derivatives are approximated by the central differencing operator, resulting in an algorithm accurate to the second order of spatial and temporal discretization Δx and Δt.

In spite of its simplicity and versatility, the FDTD method requires a relatively large number of nodes (usually 10 to 20 nodes per minimum wavelength for a problem of moderate size) in order to achieve a reasonably good accuracy [1]–[3]. This can be attributed to its relatively large linear phase error (i.e., the dispersion error), which accumulates rapidly with time [4]. If long-time solutions are required or if the problem size increases, the grid density (number of nodes per minimum wavelength) has to be increased even further. Alternatively, higher order (e.g., the fourth order) finite difference methods can be used to reduce this dispersion error [4].

Over the past two decades, another class of methods, namely the spectral methods, have been developed and applied to solve partial differential equations in fields ranging from fluid dynamics, weather prediction, to wave propagation (see, for example, [5], [6]). In contrast to the FDTD method, which uses local approximation to the spatial derivatives, the spectral methods use global functions to approximate spatial derivatives. A major advance on spectral methods was made in 1972 by Kreiss and Oliger [4] and by Orszag [7] who used trigonometric functions and Chebyshev polynomials to represent the derivatives. This method, now known as the pseudospectral method [7], [8], gains much popularity because of its superior accuracy and efficiency achieved through the fast Fourier transform (FFT) algorithm of Cooley and Tukey [9].

Another type of spectral method, the so-called k-space method, was first proposed by Bojarski [10] for scalar acoustic waves and later generalized by Liu [11], [12] to vectorial electromagnetic and elastic waves. Instead of solving the PDEs, the k-space method solves the time-domain integral equation derivable from the PDEs and uses the FFT algorithm to speed up the spatial convolution integrals. With a similar efficacy as the Fourier pseudospectral method (unfortunately not with the same popularity), the k-space method is especially useful for scattering problems. For wave equations with smoothly varying coefficients, both the Fourier pseudospectral method and the k-space method can achieve an exact spatial derivative with a grid density of only two nodes per minimum wavelength [4], [11], [12]. Fornberg has further developed the idea of viewing the Fourier pseudospectral method as a limiting case of infinite-order accurate finite-difference method [13].

Unfortunately, due to the periodicity implied by the discrete Fourier transform, both the Fourier pseudospectral method and the k-space method, if applied to unbounded media, suffer from the so-called "wraparound effect," a term used to describe the contamination of waves from other periods at late time. Therefore, to avoid this problem, the Chebyshev pseudospectral method has to be used [13], which inevitably increases the grid density require-

Manuscript received October 22, 1997; accepted February 24, 1998. This work was supported by Environmental Protection Agency under a PECASE grant CR-825-225-010, by Sandia National Laboratories under a SURP grant, and by National Science Foundation under a CAREER grant ECS-9702195.

The author is with the Klipsch School of Electrical and Computer Engineering, New Mexico State University, Las Cruces, NM 88003 (e-mail: qhliu@nmsu.edu).

ment to π nodes per minimum wavelength, and makes the CFL stability condition more stringent.

The aim of this work is to extend a method recently proposed for computational electromagnetics [14]–[16] to simulate acoustic waves in absorptive media [17]. This method combines the conventional Fourier pseudospectral method with the newly developed perfectly matched layer (PML) by Berenger [18] to eliminate the wraparound effect. Although a simple dissipative buffer zone has been used previously to reduce the wraparound effect [19], [20], it requires a large portion of the computation domain to be occupied by the buffer zone in order to reduce the reflections caused by the mismatch in wave impedances and velocities in the adjacent layers of lossy media in the buffer zone. In contrast, different layers of PMLs are matched, giving a reflectionless interface between the domain of interest and the PML buffer zone. The PML was first proposed by Berenger [18] for electromagnetic waves. Chew and Liu [21]–[23] prove that such a reflectionless PML interface also exists for elastic waves in solids in spite of the coupling between compressional and shear waves whose velocities and impedances are different. Liu and Tao [24], [25] further extend the PML to acoustic waves in absorptive media. Other applications of PML to acoustic and elastic waves can be found in [26], [27]. In a parallel development similar to [14]–]17], the Chebyshev pseudospectral method has been recently combined with the PML in [28], [29] for electromagnetic scattering problems.

We first summarize the finite difference method and Fourier pseudospectral method in Section II. Following the similar formulation for electromagnetic waves, we develop an algorithm, which has been referred to as the pseudospectral time-domain (PSTD) algorithm, combining the conventional Fourier pseudospectral method and PML in Section III for acoustic waves in absorptive media. Section IV presents numerical results in multidimensions for the validation and applications of the PSTD method. For convenience in the following discussions, FD will refer to the second-order finite-difference method, and PS will refer to the Fourier pseudospectral method.

II. FD and PS Methods

We summarize the finite difference and pseudospectral methods for partial differential equations. More details can be found in [4]–[8], [13]. To illustrate, we attempt to solve a simple first-order hyperbolic PDE:

$$\frac{\partial u(x,t)}{\partial x}+\frac{1}{c}\frac{\partial u(x,t)}{\partial t}=0,\quad x\in[0,L],\quad 0\le t \tag{1}$$

with a periodic boundary condition $u(0,t)=u(L,t)$ and an initial condition $u(x,0)=f(x)=e^{i\omega x/c}$. This PDE has an exact solution:

$$u(x,t)=e^{i\omega(x/c-t)}. \tag{2}$$

To solve this problem numerically using the FD and PS methods, both space and time are discretized. Because the difference between the two methods lies in the spatial derivative only, our discussion will be limited to the spatial discretization. If $\Delta x=L/N_x$ is used as the cell size and $x_j=j\Delta x$, $j=0,1,\ldots,N_x-1$, the second-order finite-difference approximation of the derivative is:

$$\left[\frac{\partial u(x,t)}{\partial x}\right]_{FD}\approx\frac{u(x+\Delta x,t)-u(x-\Delta x,t)}{2\Delta x}, \tag{3}$$

with a local truncation error $O(\Delta x^2)$. On the other hand, the PS method represents the derivative by a trigonometric polynomial:

$$\left[\left(\frac{\partial u(x,t)}{\partial x}\right)_{PS}\right]_{x=x_j}=\frac{1}{L}\sum_{m=-N_x/2}^{N_x/2-1}ik_m\tilde{u}(m)e^{ik_mx_j}, \tag{4}$$

where $k_m=2\pi m/L$, and $\tilde{u}(m)$ is the Fourier series:

$$\tilde{u}(m)=\Delta x\sum_{j=0}^{N_x-1}u(x_j)e^{-ik_mx_j}. \tag{5}$$

Note that each of the discrete Fourier transforms in (4) and (5) can be obtained efficiently by using a fast Fourier transform algorithm [9] with the number of operations $O(N_x\log_2 N_x)$. It is noted from the well-known Nyquist sampling theorem that the derivative in (4) is exact as long as $\omega\le\pi c/\Delta x$ (i.e., $\Delta x\le\lambda/2$ where λ is the wavelength). Therefore, even with only two nodes per wavelength, the PS method has no phase error due to the spatial discretization. However, for the FD method which gives a solution $u_{FD}(x,t)=e^{i\omega(x/c-\beta t)}$, where:

$$\beta(\omega)=\frac{\sin(\omega\Delta x/2c)}{(\omega\Delta x/2c)}, \tag{6}$$

the phase (or dispersion) error is:

$$e_{FD}(\omega)=\omega t(1-\beta). \tag{7}$$

It is seen that this dispersion error is linearly proportional to time. Hence, the FD method requires a very large N_x (i.e., very small Δx) for high frequency problems or if long-time solutions are needed [4], [8].

From above discussion, the advantage of the PS method is obvious for the PDE with a constant coefficient as only two nodes per wavelength are required. For PDEs with variable coefficients, although a complete theoretical analysis is not available, numerical results also show advantages over the FD method [8], [19], [20]. However, if the solution is discontinuous (e.g., tangential magnetic field components near a perfect conductor, or the shear stress tensor near a solid-fluid interface), higher spatial frequencies have to be included, and the Gibbs phenomena has to be addressed. We hope to report the progress on this aspect in the near future.

One major limitation of the above PS method is the spatial periodicity requirement that is to be addressed by this work. The traditional method for solving a nonperiodic problem by the pseudospectral method is to use

Chebyshev polynomials (or other orthogonal polynomials of Jacobi type) instead of the above trigonometric polynomials. The Chebyshev pseudospectral method requires π nodes per wavelength, and has a more stringent CFL stability condition [5], [13]. The use of PML in the PS method removes the wraparound effect for unbounded media, as discussed below.

III. The PSTD Algorithm for Acoustic Waves

Consider a linear, inhomogeneous, absorptive medium with space-dependent density $\rho(\mathbf{r})$, sound speed $c(\mathbf{r})$, and absorption coefficient $\gamma(\mathbf{r})$. The pressure field $p(\mathbf{r},t)$ and particle velocity $\mathbf{v}(\mathbf{r},t)$ field satisfy the basic Newton's law of motion and equation of continuity:

$$\rho\frac{\partial \mathbf{v}(\mathbf{r},t)}{\partial t} = -\nabla p, \tag{8}$$

$$\frac{\partial p}{\partial t} + \gamma(\mathbf{r})c^2(\mathbf{r})p(\mathbf{r},t) = -\rho(\mathbf{r})c^2(\mathbf{r})\nabla\cdot\mathbf{v}(\mathbf{r},t) + f_s(\mathbf{r},t), \tag{9}$$

where $f_s(\mathbf{r},t)$ is the volume source density of pressure injection rate (Pa/s). In (9), the absorption coefficient $\gamma(\mathbf{r})$ is used to characterize the absorptive loss in the medium. This absorption coefficient can be related to the attenuation coefficient $\alpha(\mathbf{r},\omega)$ by using the complex wavenumber $k(\mathbf{r},\omega) = \sqrt{\omega^2/c^2 + i\omega\gamma} = \omega/c'(\mathbf{r},\omega) + i\alpha(\mathbf{r},\omega)$, where $c'(\mathbf{r},\omega)$ is the dispersive wave velocity. In this work, the acoustic medium is assumed dispersionless so that $c(\mathbf{r})$ and $\gamma(\mathbf{r})$ are independent of frequency (however, c' and α are frequency dependent). The following algorithm, however, can be readily modified to model dispersive media.

In the traditional finite-difference simulation of acoustic waves, (8) and (9) are combined to obtain a second-order partial differential equation for the pressure field. In the explicit second-order finite-difference schemes, solving this second-order partial differential equation is more efficient than directly solving (8) and (9) because only pressure fields at the two earlier time steps are needed. However, to use the PSTD method, the PML formulation with the first-order equations is essential because most other absorbing boundary condition cannot be used to eliminate the wraparound effect.

A. The PML for Absorptive Media

To eliminate the wraparound effect, we use the newly developed PML as the absorbing boundary condition (ABC). The PML was originally proposed by Berenger [18] for electromagnetic waves. Chew and Liu [21]–[23] proved the existence of the PML for elastic waves in solids in spite of the coupling of compressional (P) and shear (S) waves whose wave impedances and velocities are different. The applications of PML for elastic and acoustic waves can be found in, for examples [21]–[27].

To introduce the PML for acoustic waves in absorptive media, we use the formulation of stretched coordinates as proposed for electromagnetic waves and elastic waves [21]–[23], [30]. With the stretched coordinates, derivative $\partial/\partial\eta$ ($\eta = x, y, z$) is changed to $e_\eta^{-1}\partial/\partial\eta = (a_\eta + i\omega_\eta/\omega)^{-1}\partial/\partial\eta$, where a_η is a real scaling factor, and ω_η represents the intrinsic loss in the PML medium [25]. With the split pressure field and source:

$$p = \sum_{\eta=x,y,z} p^{(\eta)}, \quad f_s = \sum_{\eta=x,y,z} f_s^{(\eta)}, \tag{10}$$

the partial differential equations are:

$$a_\eta\rho\frac{\partial v_\eta}{\partial t} + \omega_\eta\rho v_\eta = -\frac{\partial p}{\partial \eta}, \tag{11}$$

$$a_\eta\frac{\partial p^{(\eta)}}{\partial t} + (a_\eta\gamma c^2 + \omega_\eta)p^{(\eta)} + \omega_\eta\gamma c^2\int_{-\infty}^{t} p^{(\eta)}(\mathbf{r},t')dt' = -\rho c^2\frac{\partial v_\eta}{\partial \eta} + a_\eta f_s^{(\eta)}(\mathbf{r},t) + \omega_\eta\int_{-\infty}^{t} f_s^{(\eta)}(\mathbf{r},t')dt', \tag{12}$$

where $\eta = (x, y, z)$. Note that for the acoustic case, only the pressure field is split. There is no need to split the particle velocity $\mathbf{v}$ into $\mathbf{v}^{(\eta)}$ as in the elastic PML. This is simply because the second-rank stress tensor in the elastic case collapses into a zero-rank tensor (i.e., a scalar pressure field) in the acoustic case. Equations (11) and (12) consist of a total of six scalar equations. In addition, the third term in (12) requires three additional variables for each cell. Therefore, the memory requirement in the PML region is 4.5 times as required by a regular acoustic medium with the same dimension. This extra memory requirement in the boundary PML region is offset by the effectiveness of PML in absorbing the outgoing waves. Note also that, with the introduction of PML, there is an additional term involving the time-integrated pressure field in (12). This term represents the coupling of the loss in PML with the regular absorption loss. More details can be found in [25] for the PML for acoustic waves.

Under this PML formulation with the complex stretching variable $e_\eta = a_\eta + i\frac{\omega_\eta}{\omega}$, one can show that the reflection coefficient of an acoustic plane wave at a planar interface between two different PML layers can be made identically zero, as for the elastic waves [21]–[23]. For example, consider an interface $z = 0$ between two PML layers with the same acoustic parameters (wavenumber $k_1 = k_2 \equiv k$), and same stretching parameters $e_{1x} = e_{2x} \equiv e_x$ and $e_{1y} = e_{2y} \equiv e_y$ in x and y directions, but $e_{1z} \neq e_{2z}$ in the z direction. Assuming that a plane wave in medium 1 impinges on the interface in the (x, z) plane, the phase matching condition requires $k_{1x} = k_{2x} \equiv k_x$. From the dispersion relation $k_j^2 = k_{jx}^2/e_{jx}^2 + k_{jz}^2/e_{jz}^2$, that is $k^2 = k_x^2/e_x^2 + k_{jz}^2/e_{jz}^2$ for $j = 1, 2$, we obtain:

$$\frac{k_{1z}}{e_{1z}} = \frac{k_{2z}}{e_{2z}} = \sqrt{k^2 - k_x^2/e_x^2},$$

which make the reflection coefficient:

$$R = \frac{k_{2x}k_{1z}/e_{2x}e_{1z} - k_{1x}k_{2z}/e_{1x}e_{2z}}{k_{2x}k_{1z}/e_{2x}e_{1z} + k_{1x}k_{2z}/e_{1x}e_{2z}} = \frac{k_{1z}/e_{1z} - k_{2z}/e_{2z}}{k_{1z}/e_{1z} + k_{2z}/e_{2z}}$$

identically zero for all frequencies and all incidence angles. This conclusion also can be obtained from [23]. Therefore, the interface between these two layers are perfectly matched. Moreover, if medium 1 is regular ($e_{1z} = 1$), but medium 2 is a PML with $e_{2z} = a_{2z} + i\omega_{2z}/\omega$ where $\omega_{2z} > 0$, waves in the second medium will attenuate, providing a nonreflecting, attenuative buffer zone to eliminate the wraparound effect in the PS method.

B. The PSTD Algorithm

In the FDTD method for the first-order partial differential equations (11) and (12), a staggered grid is used where the pressure field is located at the cell center, and the velocity components are at the cell face centers [24], [25]. In contrast, in the PSTD method, pressure and particle velocity fields are all located at the cell center. This centered grid provides an important advantage over the FDTD algorithm because the material properties are not altered by the presence of the staggered grid. The temporal grid, however, is staggered because the central differencing is used for time stepping.

Therefore, if the unbounded medium is truncated into a finite computational domain with a total of $N_x \times N_y \times N_z$ cells (cell size $\Delta x \times \Delta y \times \Delta z$), and if the temporal grid is defined for $p^{(\eta)}$ at $t = n\Delta t$, while v_η is defined at $t = (n+1/2)\Delta t$, the pressure and velocity fields are denoted by:

$$p^{(\eta)}(j_x, j_y, j_z, n) \equiv p^{(\eta)}\left[\left(j_x + \frac{1}{2}\right)\Delta x, \left(j_y + \frac{1}{2}\right)\Delta y, \left(j_z + \frac{1}{2}\right)\Delta z, n\Delta t\right], \tag{13a}$$

$$v_\eta(j_x, j_y, j_z, n) \equiv v_\eta\left[\left(j_x + \frac{1}{2}\right)\Delta x, \left(j_y + \frac{1}{2}\right)\Delta y, \left(j_z + \frac{1}{2}\right)\Delta z, \left(n + \frac{1}{2}\right)\Delta t\right], \tag{13b}$$

where n is an integer, and $j_\eta = 0, \ldots, N_\eta - 1$. Furthermore, the second and third terms on the left-hand side of (12) require the averaging of their values at $t = n\Delta t$ and $t = (n+1)\Delta t$ because p is not evaluated at $t = (n+1/2)\Delta t$. This averaging has the same second-order accuracy as the central differencing used for the first term on the left-hand side of (12), and therefore does not degrade the overall accuracy in the discretization.

Using the PSTD method with this discretization, (11) and (12) become time-stepping equations:

$$v_\eta(j_x, j_y, j_z, n) = g_{1\eta} v_\eta(j_x, j_y, j_z, n-1) + g_{2\eta}\mathcal{D}_{\eta,PS}\Big[p(j_x, j_y, j_z, n)\Big], \tag{14}$$

$$p^{(\eta)}(j_x, j_y, j_z, n+1) = g_{3\eta} p^{(\eta)}(j_x, j_y, j_z, n) + g_{4\eta} p_I^{(\eta)}(j_x, j_y, j_z, n) + g_{5\eta}\mathcal{D}_{\eta,PS}\Big[v_\eta(j_x, j_y, j_z, n)\Big] + g_{6\eta} f_s^{(\eta)}\left(j_x, j_y, j_z, n + \frac{1}{2}\right), \tag{15}$$

where

$$g_{1\eta} = \frac{a_\eta/\Delta t - \omega_\eta/2}{a_\eta/\Delta t + \omega_\eta/2}, \quad g_{2\eta} = -\frac{1}{\Big(a_\eta/\Delta t + \omega_\eta/2\Big)\rho\Delta\eta}, \tag{16}$$

$$g_{3\eta} = \frac{a_\eta/\Delta t - (a_\eta\gamma c^2 + \omega_\eta)/2}{D_{\eta v}}, \quad g_{4\eta} = -\frac{\omega_\eta\gamma c^2\Delta t}{D_{\eta v}}, \tag{17}$$

$$g_{5\eta} = -\frac{\rho c^2}{D_{\eta v}}, \quad g_{6\eta} = \frac{1}{D_{\eta v}}, \tag{18}$$

$$p_I^{(\eta)}(j_x, j_y, j_z, n) = \frac{1}{2}p^{(\eta)}(j_x, j_y, j_z, 0) + \sum_{l=1}^{n} p^{(\eta)}(j_x, j_y, j_z, l), \tag{19}$$

and $D_{\eta v} = a_\eta/\Delta t + (a_\eta\gamma c^2 + \omega_\eta)/2 + \omega_\eta\gamma c^2\Delta t/2$. The PS operator $\mathcal{D}_{\eta,PS}$ on a function $u(j_\eta)$ for $\eta = x, y, z$ is defined as:

$$\mathcal{D}_{\eta,PS}\Big[u(j_\eta)\Big] = \frac{i2\pi}{N_\eta^2}\sum_{m=-N_\eta/2}^{N_\eta/2-1} m\tilde{u}(m)e^{i2\pi m j_\eta/N_\eta}, \tag{20}$$

where

$$\tilde{u}(m) = \sum_{j_\eta=0}^{N_\eta-1} u(j_\eta)e^{-i2\pi m j_\eta/N_\eta}. \tag{21}$$

Note that the operations in (20) and (21) are obtained by an FFT algorithm with a number of operations $O(N_\eta \log_2 N_\eta)$. In (15), the source f_s is assumed to be located at a regular non-PML region. In contrast to the FDTD method [25], there is no need for the material averaging in the calculations of coefficients in (16)–(18).

Equations (14) and (15) constitute a leap-frog system for v_η and $p^{(\eta)}$ ($\eta = x, y, z$). Given a particular source excitation $f_s(\mathbf{r}, t)$, this time-stepping system provides the wavefield solutions for the entire grid. The absorption of outgoing waves is achieved by the PML region that consists of several (typically 10) layers of PML materials with a tapered profile to increase the attenuation toward the outer boundary. Note that because of the periodicity in the PSTD method, the PML profile with a total of $2K$ PML cells in each direction can be distributed at either ends of the boundaries. For example, as shown in Fig. 1 for the normalized PML profile $\omega_x/\omega_{x,\max}$ in the x direction, K_1 cells of PML medium are at the left end, and $(2K - K_1)$ cells of PML medium are located at the right end of the boundaries, and K_1 can be any integer in the range $0 \le K_1 \le 2K$. Usually a quadratic profile is chosen for the PML buffer zones. In Fig. 1 and the following discussions, a normalized maximum PML attenuation coefficient $W_x = \omega_{\eta,\max}/2\pi f_c$ is defined where f_c is the center frequency of the source time function.

It is worthwhile to discuss about the implementation of finite acoustic sources in the PSTD algorithm. In (15), if the source is a point source, after spatial FFT, the well-known Gibbs phenomenon will occur because the source

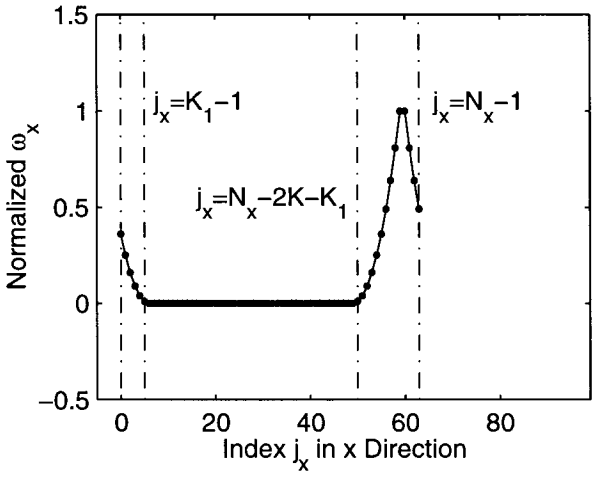

Fig. 1. A quadratically tapered PML profile for the PSTD method. Due to the periodicity, K_1 can be any integer in the range $0 \leq K_1 \leq 2K$, where 2K is the total number of PML cells.

represents a spatially discretized delta function. A simple way to eliminate this problem is to approximate the source as a spatially smoothed source occupying a volume of only a few (four to six) cells in each direction. This will avoid the inaccuracy in the FFT representation of a discrete delta function. Alternatively, one can solve for the scattered field by explicitly subtracting the known incident field due to a point source in a homogeneous medium.

Another comment is made on the PSTD algorithm regarding the smoothness of the functions under the PS operator. As can be seen from (11), (12), (14), and (15), the PS operator $\mathcal{D}_{\eta,PS}$ operates on p and v_η, the field components that are continuous across interfaces perpendicular to the $\hat{\eta}$ direction. This smoothness guarantees the effectiveness of the PSTD method even for media with material discontinuities. Therefore, for reasonably large contrasts in material properties, little Gibbs phenomenon is observed. For the extreme case where the contrast is infinity (for example, a perfectly soft boundary used to simulate an air-fluid interface), however, one of these field components is no longer continuous, and significant Gibbs phenomenon will arise. Methods are currently being investigated to mitigate this difficulty [31].

C. Dispersion Relation and Stability Condition

The dispersion analysis and stability condition of the above algorithm can be formulated for a homogeneous, nonabsorptive medium, as discussed in [15] for electromagnetic waves. The dispersion relation for the PSTD method is:

$$k = \frac{2}{c\Delta t} \sin \frac{\omega \Delta t}{2}, \tag{22}$$

where $k = \sqrt{k_x^2 + k_y^2 + k_z^2}$. Assuming $\Delta x = \Delta y = \Delta z$, the CFL stability condition is:

$$\frac{c\Delta t}{\Delta x} \leq \frac{2}{\sqrt{D}\pi}, \tag{23}$$

where D is the dimensionality of the problem. Given the same cell size Δx, the stability criterion in (23) for the PSTD algorithm is more stringent than that for the FDTD method by a factor of $\pi/2 \approx 1.5708$. However, considering the fact that for the same accuracy, the FDTD method requires much smaller Δx than the PSTD algorithm, the time step for the PSTD algorithm can be chosen larger than that in the FDTD method. In practice, the choice of Δt in the PSTD method is usually dictated by the accuracy consideration instead of stability consideration.

IV. Numerical Results

We have implemented the PSTD algorithm with the perfectly matched layers as the absorbing boundary condition for one, two, and three dimensions. Unlike the continuous case, some reflection will occur at the discretized PML interface. This reflection increases with the contrast in the coordinate stretching variables. Therefore, to minimize the reflection from the PML layers, we choose a quadratic or linear profile for the PML coordinate-stretching variables. Typically we use 10 cells of perfectly matched layers at the computational edge on each side (i.e., $K = K_1 = 10$ in Fig. 1).

In the following examples, a monopole source is used to excite the acoustic wavefield. The time function $f_s(t)$ of the source is the first derivative of the Blackman-Harris window function [15], [16]. Unless otherwise stated, the center frequency of the source will be $f_c = 20$ kHz.

A. A Large 1-D Problem

The purpose of this example is to compare the accuracy of the PSTD and FDTD methods for large-scale problems. Fig. 2(a) shows a three-layer problem with $\rho_j = 2200$, 2500, 2200 kg/m^3, $c_j = 2500$, 3500, 2500 m/s, and $\gamma_j = 0$ for $j = 1, 2, 3$. An infinite sheet of monopole source is located at $x = 1.6$ m, and the receiver is located at $x = 25$ m. The center frequency of the source is $f_c = 20$ kHz, and the size of the problem is $512\lambda_{\min}$ where $\lambda_{\min} = 0.05$ m is the minimum wavelength at the highest frequency considered ($f_{\max} = 2.5 f_c$). The time step is chosen as $\Delta t = 0.2$ μs so that the error due to the temporal discretization is small.

Fig. 2(b) shows three sets of pressure waveforms at the receiver location: the PSTD result with a grid density of $GD = 2$; the FDTD results with a grid density of $GD = 16$, and $GD = 32$. Although the PSTD result is very accurate, the FDTD results, even with 32 nodes per wavelength, have noticeable dispersion errors. The dispersion errors are displayed in Figs. 2(c) and (d) for the FDTD and PSTD methods. One observes that with $GD = 32$, the maximum dispersion error for the FDTD method is about 10%, and that for the PSTD method is 1% with $GD = 2$. Furthermore, this dispersion error for PSTD can be reduced by decreasing Δt. In contrast, to reduce the error in the FDTD results, both Δx and Δt have to be reduced.

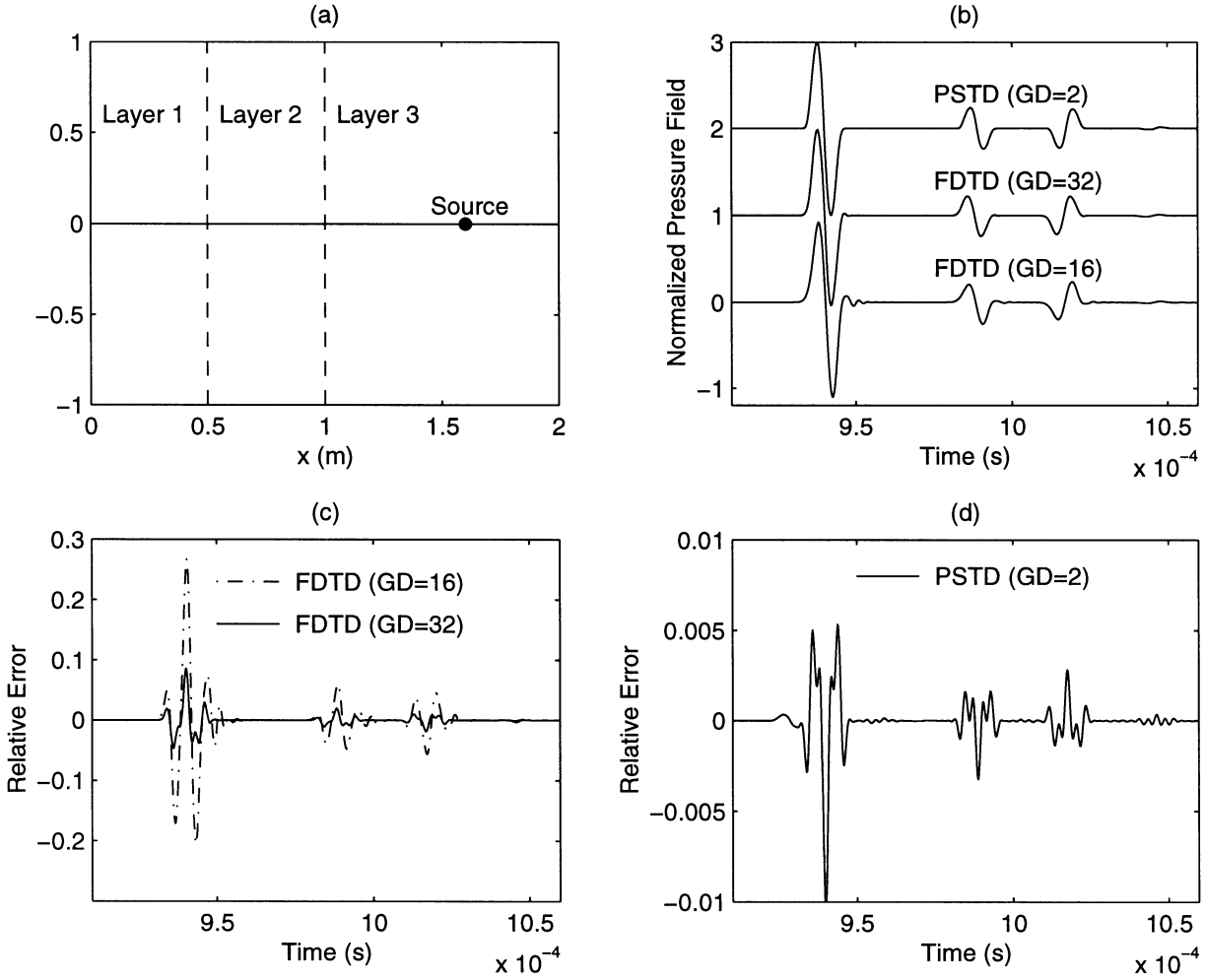

Fig. 2. PSTD and FDTD results for a large-scale 1-D problem of size $512\lambda_{\min}$.

For the FDTD method to produce a result accurate to within 1%, it is expected that the grid density has to be at least 64 for this large-scale problem. It means that it requires at least 32 times more computer memory, and about the same factor more CPU time than the PSTD method. As an extrapolation to a multidimensional problem of size $512\lambda_{\min}$ in each linear dimension, the PSTD method is at least 32^D times more efficient than the FDTD method, where D is the dimensionality of the problem.

B. A 2-D Homogeneous Medium

The purpose of this study is twofold. First, the PSTD method will be validated by an analytical result. Second, the choice of the PML profile will be investigated.

The properties of the homogeneous medium are $\rho = 2200$ kg/m^3, $c = 2500$ m/s, and $\gamma = 0$ in two dimensions. A monopole line source is located at $(x, y) = (0.8, 0.8)$ m, the center of the computational domain with $N_x \times N_y = 64 \times 64$, $\Delta x = \Delta y = 0.5\lambda_{\min} = 0.025$ m. The time step is chosen as $\Delta t = 0.3$ μs. The pressure field p is calculated at $(x, y) = (1.25, 0.8)$ m. To verify the PSTD result, an analytical solution is obtained by inverse Fourier transforming the following frequency-domain solution:

$$p(\mathbf{r}, \omega) = \frac{\omega}{4c^2} H_0^{(1)}(kr) F_s(\omega), \tag{24}$$

where $F_s(\omega)$ is the Fourier transform of $f_s(t)$, and $k = \sqrt{\omega^2/c^2 + i\omega\gamma}$.

Fig. 3(a) shows the comparison between the PSTD result (where $W_x = 1$ is used) and the analytical solution. Excellent agreement is found between the two solutions. To obtain the reflected waves off the boundary, we use the PSTD method to simulate a reference model whose computational domain is so large that the reflected waves do not appear in the time interval of interest. The reflected waves in our model of interest are then obtained by subtracting the reference waves from the total waves in Fig. 3(a). To characterize the performance of the PML absorbing boundary condition, we choose a series of different values of PML attenuation coefficient W_x. Figs. 3(b) and (c) show the reflected waves corresponding to $W_x = 0.5$, 1.0, and 2.0. The maximum reflected amplitudes for these cases are -41.5 dB, -81.3 dB, and -77.4 dB, respectively. For this particular problem, the case with $W_x = 1$ gives the smallest reflection. As expected, the optimal W_x depends on the sound speed of the medium. In general, for a medium with

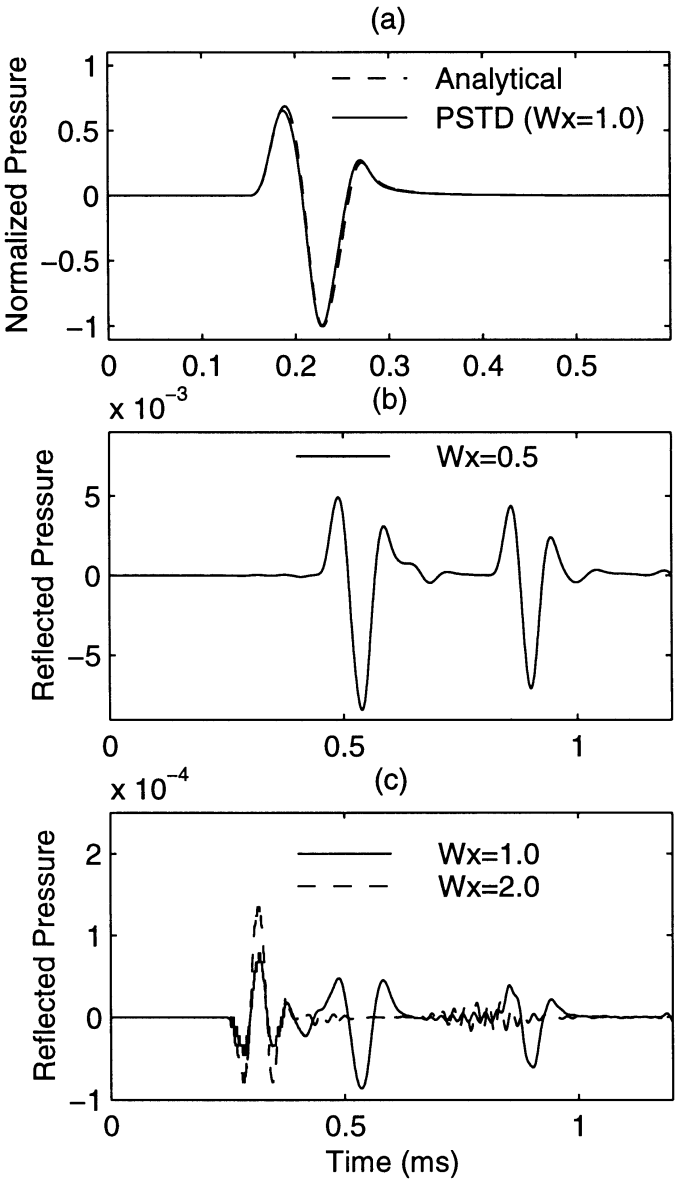

Fig. 3. PSTD and analytical results for a 2-D homogeneous medium. (a) Pressure field at $r = 0.45$ m. (b) Reflected waves for $W_x = 0.5$. (c) Reflected waves for $W_x = 2.0$ and $W_x = 1.0$.

sound speed c, the choice $W_x = c/2500$ gives satisfactory results.

C. 2-D Inhomogeneous Half Space

In this example, we compare the 2-D PSTD method with the FDTD method for a 2-D inhomogeneous half-space. The two acoustic media with $\rho_1 = 2200$ kg/m^3, $c_1 = 2500$ m/s, $\gamma_1 = 0$, and $\rho_2 = 2500$ kg/m^3, $c_2 = 3500$ m/s, $\gamma_2 = 0$, are separated by an interface at $y = 0.925$ m. A monopole source is located at $(x, y) = (0.8, 0.8)$ m, and 19 receivers are located at $(x_j, y_j) = (1.3, 0.3 + 0.05j)$ m $(j = 1, \ldots, 19)$. The computational domain $x \in [0, 1.6]$, $y \in [0, 1.6]$ m is discretized by a uniform grid. The PSTD method uses a grid of $N_x \times N_y = 64 \times 64$ and $\Delta x = \Delta y = \lambda_{\min}/2 = 0.025$ m, and the FDTD method uses a grid of $N_x \times N_y = 256 \times 256$ and $\Delta x = \Delta y = \lambda_{\min}/8 = 0.00625$ m. A small time step $\Delta t = 0.3$ μs is used so that accuracy and stability requirements are satisfied for both methods. For brevity, the geometry is now shown here, but it is the same as in Fig. 4(a) below except that the two rectangular objects are absent.

In Fig. 5(a) the waveforms at the receiver array are displayed for the PSTD and FDTD results. The good agreement between the two sets of results can be better observed in Fig. 5(b) for the waveforms at the 5-th receiver in spite of the fact that only two nodes per minimum wavelength are used in the PSTD method. For this problem of moderate size of $32\lambda_{\min} \times 32\lambda_{\min}$, the FDTD methods uses 16 times more memory and CPU time. For problems of larger scales (or equivalently for longer propagation time), a much finer grid has to be used in the FDTD method, significantly increasing its computational cost.

D. Objects Buried Under a Half Space

To illustrate the applications of the PSTD method, acoustic wave interaction with two objects buried under the half space in the last example is simulated. The geometry is shown in Fig. 4(a), and the two objects have the same material parameters $\rho = 2800$ kg/m^3, $c = 4500$ m/s, $\gamma = 0$. The discretization for the PSTD method is the same as that in the last example.

Fig. 4(b) shows the total pressure field at the receiver array. In order to show the effects of the scattered field off the two objects, we perform a simulation for the half space without the two objects and call this pressure field the "incident field," which is subtracted from the total field to obtain the scattered field of the objects. (Note that this "incident field" is actually calculated by the last example.) Figs. 4(c) and (d) show the incident and scattered waves, respectively, at the receiver array. The maximum amplitude of the scattered field is 31.6% of the maximum amplitude of the total field.

The propagation of acoustic waves can be observed more clearly with the wavefield snapshots. From the above simulations, we obtain the snapshots for the total field and incident field. Then the snapshots for the scattered field are obtained by subtracting the incident field from the total field, as shown in Fig. 6. Note that the dynamic range is reduced from the third plot by a factor of $1.5^{|j-3|}$ $(j = 1, \ldots, 15)$ for all plots in order to show the wavefield clearly.

E. Three-Dimensional Effects

In the above 2-D examples, the source is a monopole line source with an infinite extend in z direction. Similarly, the medium is assumed invariant in z direction. In reality, measurements are performed in three dimensions. To study the 3-D effects, we simulate a similar problem as in the last example. The two half spaces are exactly the same, but the two objects are finite in z direction: the object on the left occupies $0.4 \leq z \leq 0.55$ m, and the second

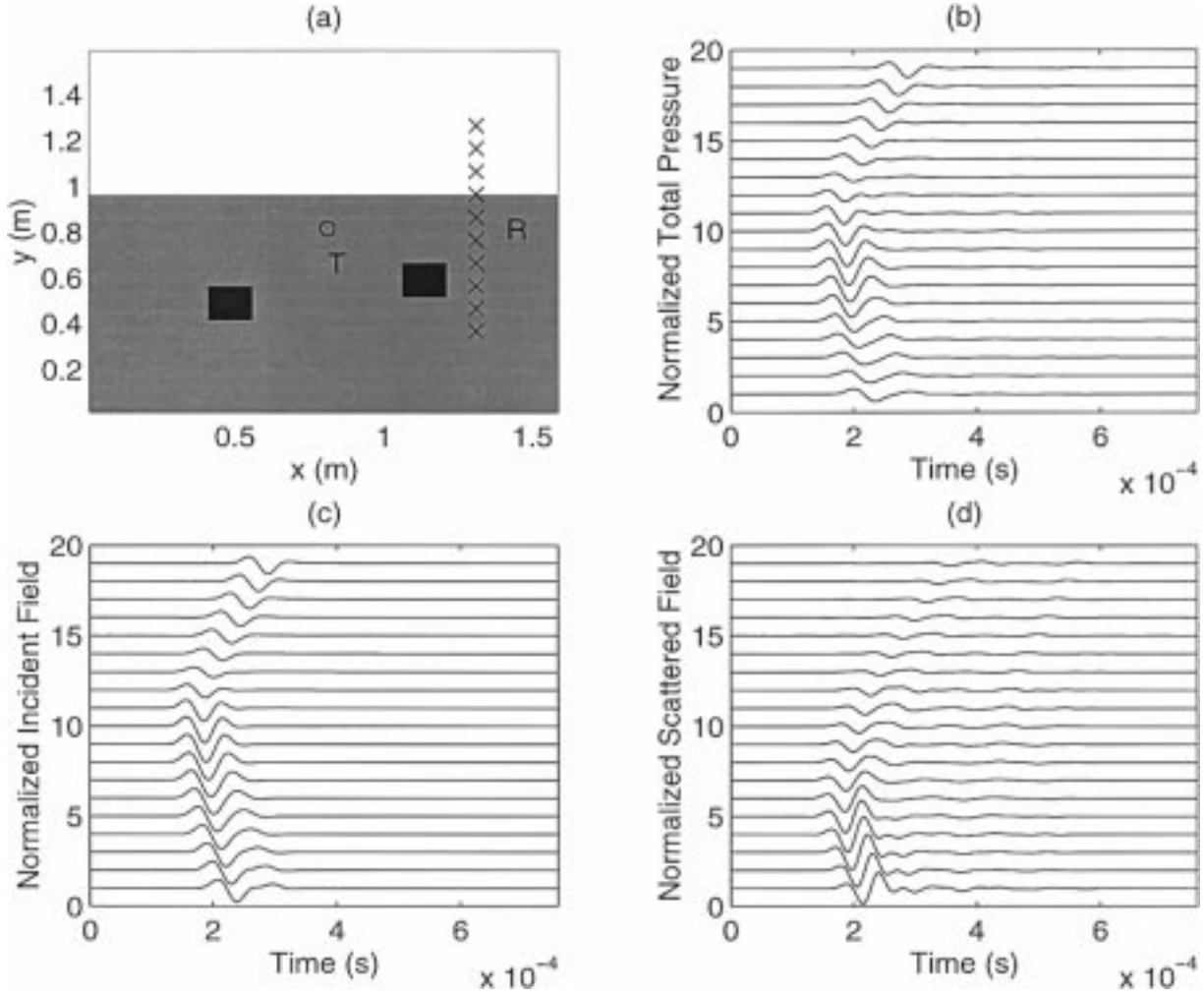

Fig. 4. Two objects in a 2-D half space. (a) Geometry, (b) total pressure field, (c) incident pressure field, (d) scattered field.

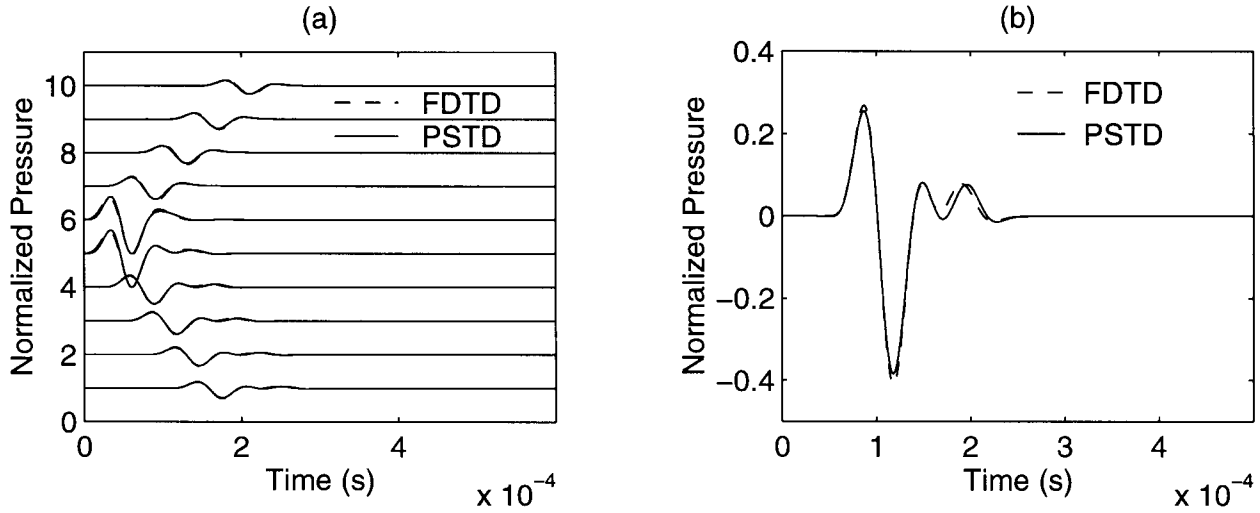

Fig. 5. Comparison of PSTD algorithm (grid density: 2) and FDTD results (grid density: 8) for a half space. (a) Waveforms at the receiver array, (b) waveforms at the 5th receiver.

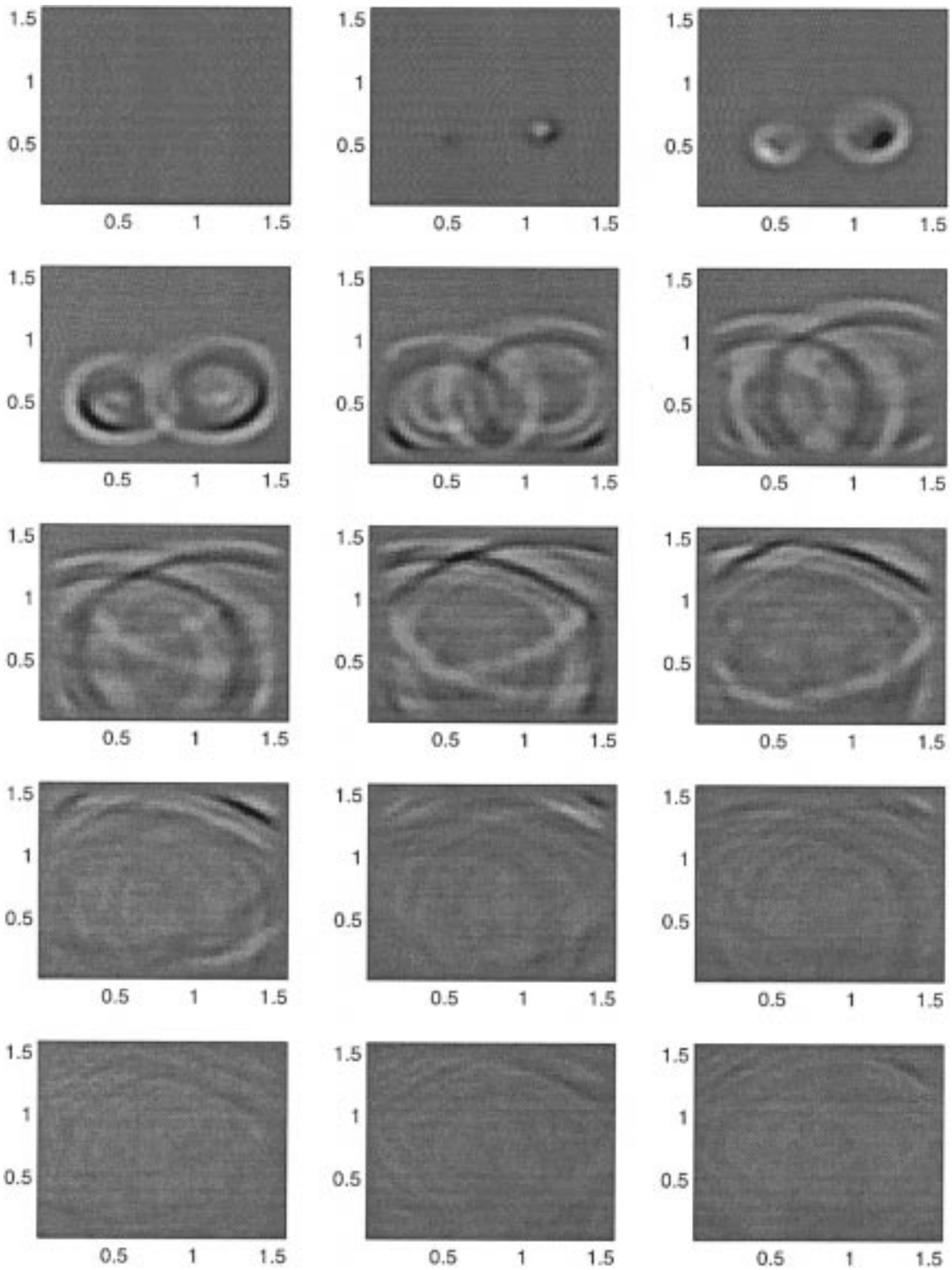

Fig. 6. From left to right and top to bottom, snapshots of the scattered pressure field in the PSTD algorithm for Fig. 4(a) at time steps $n = 200j$ $(j = 1, \ldots, 15)$ where $\Delta t = 0.3$ μs. The dynamic range is reduced from the third figure by a factor of $1.5^{[j-3]}$ $(j = 1, \ldots, 15)$.

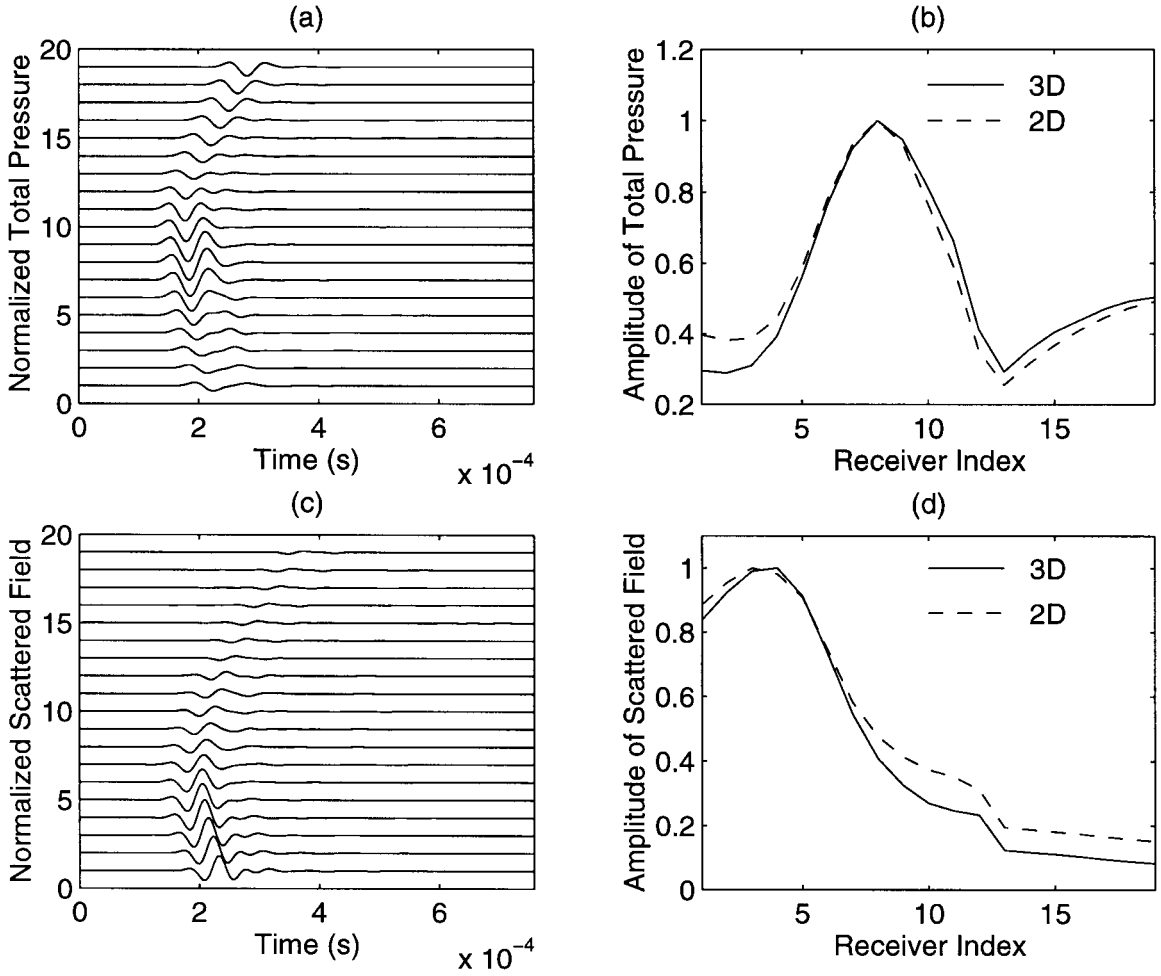

Fig. 7. The 3-D effects with a finite source and finite scatterers. (a) Total pressure field, (b) amplitude of total field as a function of receiver locations, (c) scattered field, (d) amplitude of scattered field as a function of receiver locations.

object occupies $0.65 \leq z \leq 0.95$ m. The point monopole source and the receiver array are located at the mid-plane ($z = 0.8$ m). The problem is simulated by using the 3-D PSTD program with $N_x \times N_y \times N_z = 64 \times 64 \times 64$ and all other discretization parameters are the same as in the last example.

Figs. 7(a) and (b) show the 3-D effects in the total field at the receiver array. It is observed from the amplitude plot in Fig. 7(b) that inside the lower half space away from the interface, as expected, the field decays faster in 3-D than in 2-D. Near the interface, however, the field in 3-D decays more slowly due to the wave interference with the interface. However, for the scattered field, the amplitude decays faster in 3-D everywhere, as shown in Figs. 7(c) and (d). This is because the interference has been subtracted out since it is part of the incident field. (Recall that the incident field was defined earlier as the field without the objects, but with the interface.)

For this 3-D problem, the FDTD method would have required a grid at least of size $N_x \times N_y \times N_z = 256 \times 256 \times 256$, making the memory requirement at least 64 times that in the PSTD method.

F. Effects of Intrinsic Attenuation

Because the PSTD method formulated in this work is for an absorptive medium, it can be used to investigate the effects of intrinsic attenuation. As an example, we simulate the same model as in Fig. 7, except that the lower half space is now absorptive with $\gamma = 0.001$ s/m^2. The total field and the scattered field are shown in Figs. 8(a) and (c). Their amplitudes are compared in Figs. 8(b) and (d) with the lossless case in the last example. Note that the amplitude plots are normalized with respect to the lossless case. Significant effects of the intrinsic attenuation are observed in the lossy medium. Therefore, it is important for a numerical method to include the intrinsic absorption of the medium in its model.

V. Conclusions

A pseudospectral time-domain (PSTD) algorithm is proposed to simulate transient acoustic wave propagation in multidimensional, inhomogeneous, absorptive media. The algorithm is based on the combination of the Fourier pseudospectral method and the perfectly matched layer for acoustic media. The PSTD method uses trigono-

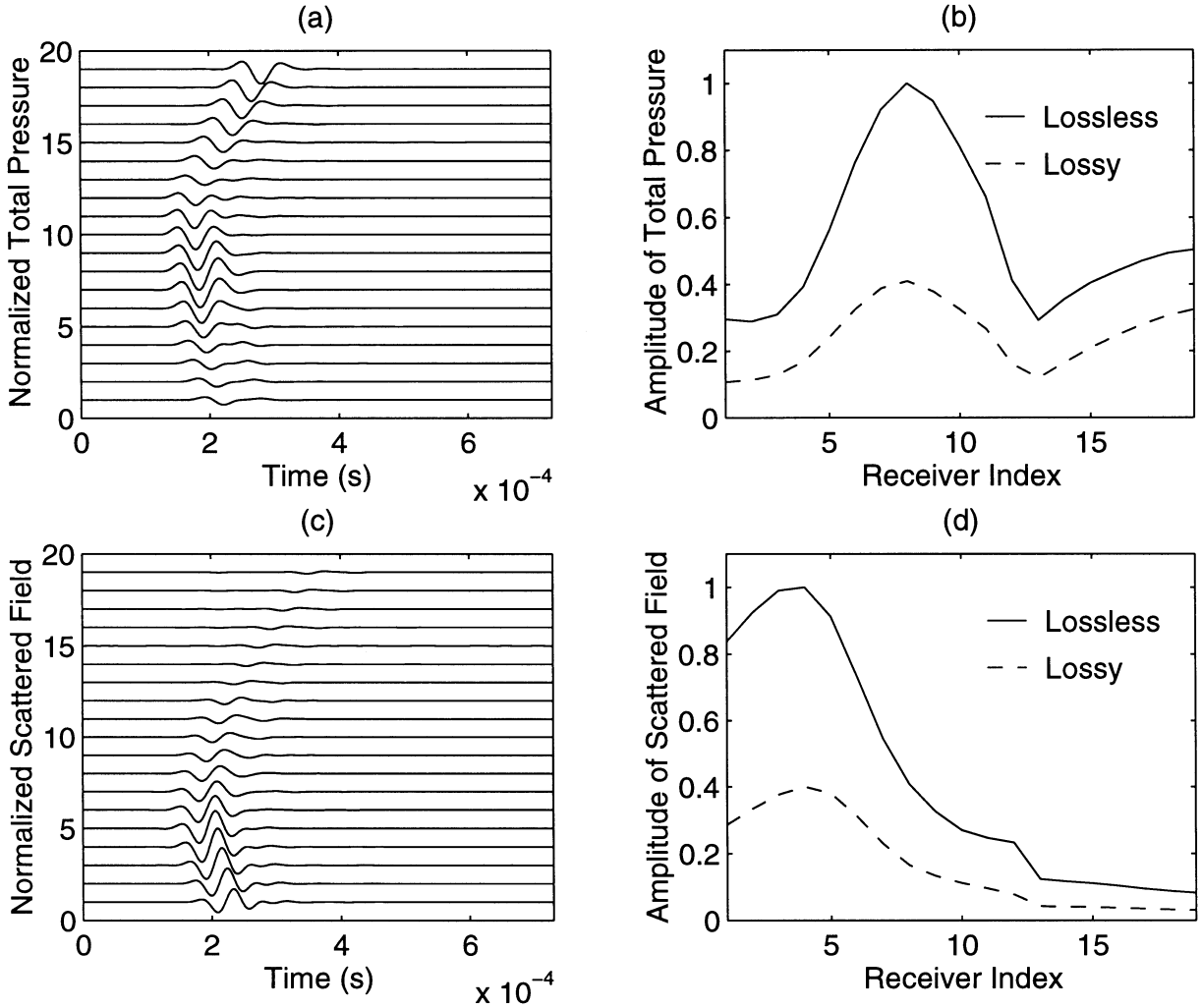

Fig. 8. The effect due to absorption in the second half space. (a) Total pressure field, (b) amplitude of total field as a function of receiver locations, (c) scattered field, (d) amplitude of scattered field as a function of receiver locations.

metric functions, through an FFT algorithm, to represent the spatial derivatives in partial differential equations, resulting in an infinite order of accuracy (up to the spatial Nyquist frequency) in the spatial derivatives. Therefore, unlike the traditional FDTD method, the PSTD method has no dispersion error associated with the approximation of spatial derivatives. The only numerical dispersion error is in the approximation of temporal derivatives, which can always be reduced by choosing a smaller time step. The wraparound effect that limits the traditional Fourier pseudospectral method to periodic problems has been eliminated by the perfectly matched layers. We have implemented the PSTD algorithm for 1-D, 2-D, and 3-D problems. As shown by numerical results, a high accuracy is maintained in the PSTD algorithm even when only two cells per minimum wavelength are used in the discretization, saving a significant amount of computer memory and CPU time. As easily seen, however, one major limitation of the method is the requirement for a uniform grid as dictated by the use of the FFT algorithms. Further investigation in this problem is underway, and we hope to report the progress in the near future.

References

[1] K. S. Yee, "Numerical solution of initial boundary value problems involving Maxwell's equations in isotropic media," *IEEE Trans. Antennas Propagat.*, vol. AP-14, pp. 302–307, 1966.

[2] K. S. Kunz and R. J. Luebbers, *Finite Difference Time Domain Method for Electromagnetics*. Boca Raton, FL: CRC Press Inc., 1993.

[3] A. Taflove, *Computational Electrodynamics: The Finite Difference Time Domain Method*. Norwood, MA: Artech House, 1995.

[4] H.-O. Kreiss and J. Oliger, "Comparison of accurate methods for the integration of hyperbolic equations," *Tellus*, vol. 24, pp. 199–215, 1972.

[5] D. Gottlieb and S. A. Orszag, *Numerical Analysis of Spectral Methods*. Philadelphia: SIAM, 1977.

[6] C. Canuto, M. Y. Hussani, A. Quarteroni, and T. Zang, *Spectral Methods in Fluid Dynamics*. New York: Springer-Verlag, 1988.

[7] S. A. Orszag, "Comparison of pseudospectral and spectral approximation," *Stud. Appl. Math.*, vol. 51, pp. 253–259, 1972.

[8] B. Fornberg, "On a Fourier method for the integration of hyperbolic equations," *Soc. Industr. Appl. Math. J. Numer. Anal.*, vol. 12, pp. 509–528, 1975.

[9] J. W. Cooley and J. W. Tukey, "Algorithm for the machine computation of complex Fourier series," *Math. Comput.*, vol. 19, pp. 297–301, 1965.

[10] N. N. Bojarski, "The k-space formulation of the scattering problem in the time domain," *J. Acoust. Soc. Amer.*, vol. 72, pp. 570–584, 1982.

[11] Q. H. Liu, "Transient electromagnetic modeling with the generalized k-space (GKS) method," *Microwave Opt. Tech. Lett.*, vol. 7, no. 18, pp. 842–848, 1994.
[12] ——, "Generalization of the k-space formulation to elastodynamic scattering problems," *J. Acoust. Soc. Amer.*, vol. 97, no. 3, pp. 1373–1379, 1995.
[13] B. Fornberg, *A Practical Guide to Pseudospectral Methods*. New York: Cambridge Univ. Press, 1996.
[14] Q. H. Liu, "A spectral-domain method with perfectly matched layers for time-domain solutions of Maxwell's equations," in URSI Meeting, Baltimore, MD, July 1996.
[15] ——, "The PSTD algorithm: A time-domain method requiring only two cells per wavelength," *Microwave Opt. Tech. Lett.*, vol. 15, no. 3, pp. 158–165, 1997.
[16] ——, "The pseudospectral time-domain (PSTD) method: A new algorithm for solutions of Maxwell's equations," *Int. IEEE/AP-S Symp. Digest*, pp. 122–125, Montreal, Canada, July 1997.
[17] ——, "The PSTD algorithm: A time-domain method combining the pseudospectral technique and perfectly matched layers," *J. Acoust. Soc. Amer.*, vol. 101, pt. 2, p. 3182, May 1997.
[18] J.-P. Berenger, "A perfectly matched layer for the absorption of electromagnetic waves," *J. Comput. Phys.*, vol. 114, pp. 185–200, 1994.
[19] C. Cerjan, D. Kosloff, R. Kosloff, and M. Reshef, "A nonreflecting boundary condition for discrete acoustic and elastic wave equations," *Geophysics*, vol. 50, no. 4, pp. 705–708, 1985.
[20] R. Kosloff and D. Kosloff, "Absorbing boundaries for wave propagation problems," *J. Comput. Phys.*, vol. 63, pp. 363–376, 1986.
[21] W. C. Chew and Q. H. Liu, "Perfectly matched layers for elastodynamics: A new absorbing boundary condition," *Schlumberger-Doll Res. Tech. Rep.*, GEO-002-95-26, Aug. 1995.
[22] ——, "Using perfectly matched layers for elastodynamics," *Proc. IEEE Antennas Propagat. Soc. Intl. Symp.*, vol. 1, 1996, pp. 366–369.
[23] ——, "Perfectly matched layers for elastodynamics: A new absorbing boundary condition," *J. Comput. Acoust.*, vol. 4, no. 4, pp. 72–79, 1996.
[24] Q. H. Liu and J. Tao, "Perfectly matched layers for acoustic waves in viscous media: Applications to underwater acoustics," *J. Acoust. Soc. Amer.*, vol. 101, no. 5, pt. 2, p. 3182, May 1997.
[25] ——, "The perfectly matched layer (PML) for acoustic waves in absorptive media," *J. Acoust. Soc. Amer.*, vol. 102, no. 4, pp. 2072–2082, 1997.
[26] F. D. Hastings, J. B. Schneider, and S. L. Broschat, "Application of the perfectly matched layer (PML) absorbing boundary condition to elastic wave propagation," *J. Acoust. Soc. Amer.*, vol. 100, no. 5, pp. 3061–3069, 1996.
[27] X. Yuan, D. Borup, J. W. Wiskin, M. Berggren, R. Eidens, and S. A. Johnson, "Formulation and validation of Berenger's PML absorbing boundary for the FDTD simulation of acoustic scattering," *IEEE Trans. Ultrason., Ferroelect., Freq. Contr.*, vol. 44, pp. 816–822, 1997.
[28] B. Yang, D. Gottlieb, and J. S. Hesthaven, "On the use of PML ABC's in spectral time-domain simulations of electromagnetic scattering," in *Proc. ACES 13th Annual Review of Progress in Applied Computational Electromagnetics*, Monterey, CA, 1997, pp. 926–933.
[29] ——, "Spectral simulations of electromagnetic waves scattering," *J. Comput. Phys.*, vol. 134, pp. 216–230, 1997.
[30] W. C. Chew and W. H. Weedon, "A 3D perfectly matched medium from modified Maxwell's equations with stretched coordinates," *Microwave Opt. Tech. Lett.*, vol. 7, pp. 599–604, 1994.
[31] Q. H. Liu and N. Nguyen, "An accurate algorithm for nonuniform fast Fourier transforms (NUFFT)," *IEEE Microwave Guided Wave Lett.*, vol. 8, no. 1, pp. 18–20, 1998.

Qing Huo Liu (S'88–M'89–SM'94) received the B.S. and M.S. degrees in physics from Xiamen University, China, in 1983 and 1986, respectively, and the Ph.D. degree in electrical engineering from the University of Illinois at Urbana-Champaign in 1989.

From September 1986 to December 1988, Dr. Liu was a research assistant in the Electromagnetics Laboratory at the University of Illinois at Urbana-Champaign. From January 1989 to February 1990 he was a postdoctoral research associate at the same laboratory. From 1990 to 1995 he was a research scientist and program leader with Schlumberger-Doll Research, Ridgefield, CT. Since October 1995 he has been an associate professor at the Klipsch School of Electrical and Computer Engineering, New Mexico State University, Las Cruces, New Mexico.

His research interest has been in electron paramagnetic resonance spectroscopy, microstrip antenna applications, electromagnetic wave propagation in inhomogeneous media, geophysical subsurface sensing, transient electromagnetics, inverse scattering, and elastic wave propagation.

Dr. Liu is a member of Phi Kappa Phi, Tau Beta Pi, SEG, a full member of U.S. National Committee of URSI Commisions B and F, and a Senior Member of IEEE. Currently he serves as an Associate Editor for *IEEE Transactions on Geoscience and Remote Sensing*. He received a Presidential Early Career Award for Scientists and Engineers (PECASE) from the National Science and Technology Council (NSTC) and an Early Career Research Award from the Environmental Protection Agency in 1996, and a CAREER Award from the National Science Foundation in 1997.